express
polymer letters

Research article

Development of tri-layer antioxidant packaging systems based on recycled PLA/sodium caseinate/recycled PLA reinforced with lignocellulosic nanoparticles extracted from yerba mate waste

Marina Patricia Arrieta[1,2]*, Freddys Beltran*[1,2], *Sara Soledad Abarca de las Muelas*[1], *Gerald Gaspar*[1], *Rafael Sanchez Hernandez*[3], *Maria Ulagares de la Orden*[2,4], *Joaquin Martinez Urreaga*[1,2]

[1]Departamento Ingeniería Química Industrial y Medio Ambiente, Universidad Politécnica de Madrid, E.T.S.I. Indsustriales, 28006 Madrid, Spain
[2]Grupo de Investigación: Polímeros, Caracterización y Aplicaciones (POLCA)
[3]Molecular Spectroscopy Line, Thermo Fisher Scientific S.L.U. Avenida de la Vega, 1 Edificio 1, 28108 Alcobendas, Spain
[4]Departamento Química Orgánica I, Universidad Complutense de Madrid, Facultad de Óptica y Optometría, 28037 Madrid, Spain

Abstract. Tri-layer films based on glycerol-plasticized sodium caseinate film (SC) as the middle layer and two outer layers of mechanically recycled poly(lactic acid) (RPLA) were successfully developed. Additionally, the internal RPLA-based layer was loaded either with 1 or 3 wt% of lignocellulose nanoparticles extracted from yerba mate waste (YMNs) to obtain antioxidant-active packaging formulations. YMNs were also surface modified with a surfactant to increase the interfacial adhesion and improve their dispersion into the polymeric matrix. The tri-layer system composed of YMNs loaded nanocomposites (RPLA/SC/RPLA-YMN1 and RPLA/SC/RPLA-YMN3) exhibited an improved oxygen barrier compared to the non-reinforced system counterpart (RPLA/SC/RPLA). The high water vapor permeability of SC was reduced in tri-layer systems, ascribed to the protection of the middle SC layer by the hydrophobic RPLA layers at both sides. The improved performance of all these properties was ascribed to the good adhesion between PLA and SC layers, ascribed to hydrogen bonding interactions. Furthermore, the obtained tri-layer structures showed effective antioxidant ability for fatty food, as it was demonstrated by release studies conducted in a fatty food simulant and further analysis of the radical-scavenging activity showing good antioxidant properties (RPLA/SC/RPLA-YMN1 = 36.8±2.5 GA mg/dm^2 film and RPLA/SC/RPLA-YMN3 = 81.1±2.5 Gallic Acid mg/dm^2 film). Finally, the tri-layer films were disintegrated under composting conditions in 17 days. Thus, the results show the potential of the mechanical recycling process of PLA as a sustainable alternative to revalorizing PLA waste, while the revalorization of yerba mate waste shows its interest by easily providing the materials with antioxidant properties. Finally, the tri-layer bio-based and biodegradable active formulations resulted in interesting materials for fatty foodstuffs.

Keywords: biodegradable polymers, lignocellulosic nanoparticles, recycling, nanocomposites, food packaging

1. Introduction

The great awareness to diminish the consumption of non-renewable resources along with reducing the accumulation of plastic waste after their useful life has led to a growing tendency to replace conventional petroleum-based plastic materials with biobased

and biodegradable polymers particularly in short-term applications such as food packaging [1–3]. Among biobased and biodegradable plastics, poly(lactic acid) (PLA) has been positioned in the packaging market as the most used biopolymer for films for food packaging applications, thanks to its many advantages such as availability in the market at a competitive cost, ease of processing with the usual thermoplastic technology already available in the plastic processing industry, high transparency, recyclability as well as high rate of disintegration in composting conditions [4–6]. However, the use of PLA as a film for food packaging is restrained due to the fact that PLA suffers some limitations such as low thermal and mechanical resistance as well as poor gas barrier performance [6, 7]. It is known that the crystalline phase has a significant influence on the permeation and mechanical performance, and this is why a number of research and industrial efforts have been focused on increasing PLA crystallinity to extend the PLA-based films applications in the food packaging field *i.e.*, blending or copolymerization with more crystalline polymers, developing composites and/or nanocomposites as well as the development of multilayer packaging systems [6]. In this regard, the mechanical recycling of PLA has gained interest as a scalable and cost-effective solution to manage PLA waste, offering the opportunity to give PLA more than one life before being discarded for pyrolysis or composting [8–10]. Although the degradation of PLA polymeric matrix during service as well as during reprocessing led to a reduction of the molecular weight and a consequent detriment on the mechanical properties of the recycled PLA final materials, recycled PLA shows increased crystallinity in comparison with virgin PLA [10]. In fact, in previous work, it has been observed that the mechanical recycling process of PLA films showed a reduction of the number average molecular weight (M_n) of around 12%, determined by gel permeation chromatography (GPC) [11]. Moreover, the shorter PLA polymer chains not only favor the crystallization of PLA [12] but also provide recycled PLA with more reactive end-chain groups, interesting for increasing the compatibility of PLA with other polymeric layers in multilayer packaging materials. In fact, oligomers of PLA, oligomeric lactic acid (OLA), have been used as PLA plasticizers with the aim of increasing the compatibility between different layers in PLA-based multilayer packaging formulations [13].

In most multilayer packaging formulations, the outer layers are made of water barrier polymers with good mechanical performance, while the inner layers usually consist of materials that provide good gas barrier properties [14, 15]. In this sense, agro-polymers such as proteins and polysaccharides are interesting as reinforcing fillers for developing PLA-based nanocomposites as well for developing inner layers for sustainable multilayer PLA-based packaging materials [7]. Delamination of each individual layer is frequently observed in multilayer systems when the polymeric layers are incompatible. Thus, surface chemical modifications or the addition of compatibilizers are frequently proposed to improve the adhesion between polymeric layers. In this context, caseinates are of particular interest since they are considered natural bioadhesives that offer advantageous properties for films production since proteins are able to form networks and show good elasticity while possessing good barrier performance against oxygen, carbon dioxide, and aroma compounds, making them ideal candidates for food packaging [16–18]. Although caseinates lead to hydrophilic films, having much higher water sensitivity than PLA and thus lower barrier performance to water vapor [7], they are interesting for internal layers in multilayer packaging formulations [19].

At the same time, the valorization of agro-food waste has gained considerable interest in the plastic processing industry to develop more sustainable plastic formulations to be aligned with the Circular Bioeconomy concept [20]. Interesting bioactive compounds can be extracted from several agro-food wastes and further used as additives in the plastics processing industry to provide the final materials with interesting functional properties such as antioxidant or antibacterial ability [20–22]. The incorporation of active compounds into the polymeric matrix allows the commercialization of chemical preservative-free food products. Yerba mate (*Ilex paraguairiensis*, aint Hilaire) is an important commercial tree original from the subtropical region of South America, which naturally grows in a narrow region within Argentina, Brazil, and Paraguay [23]. Yerba mate is industrialized to get the commercial product from the dry leaves used to make a very popular infusion drink in hot water popularly known in Argentina, Paraguay, and Uruguay as 'mate' [23, 24] and in Brazil as 'chimarrão' [25]. The infusion of yerba mate is generally consumed because of its

well-known beneficial antioxidant properties provided by the polyphenols' high content compounds such as lignin, caffeic acid, and chlorogenic acid [24, 26]. Its elevated consumption leads to the generation of high amounts of yerba mate waste, mainly because after being consumed as an infusion, it is wasted, lacking any kind of revalorization [24, 27]. In this regard, yerba mate waste has been used for the extraction of lignocellulosic nanoparticles showing interesting antioxidant activity even when being extracted from the yerba mate waste [24]. In fact, the total polyphenol content of pristine yerba mate extract is between 50 and 70 mg/g of gallic acid/g yerba mate [26, 28], while the total polyphenolic content of yerba mate nanoparticles is around 40 mg/g of gallic acid/g yerba mate [24]. Yerba mate nanoparticles extracted from yerba mate waste (YMNs) have shown their effectiveness to improve the thermal stability and the mechanical performance of neat PLA [24] as well as the thermal stability and the oxygen barrier performance of recycled PLA [11, 29]. Although YMNs have proven their great potential to improve PLA performance, the high amount of –OH in the lignocellulose nanoparticles induces high attraction between them, leading to nanocellulose agglomeration, particularly during the freeze-drying process, making difficult the homogenous dispersion of nanoparticles into the PLA matrix [30–32].

The homogeneous dispersion of high polarity lignocellulosic nanoparticles into the hydrophobic PLA matrix could be favored by functionalizing the nanoparticles surface. This is why many research efforts are focused on the improvement of lignocellulosic nanoparticles dispersion by modification of their surface by both chemical and/or physical modifications [30]. The chemical modification is usually performed by grafting polymer chains (*i.e.*: PLA or poly(ε-caprolactone) (PCL)) at the surface of the nanoparticles through a 'grafting from' approach [33], while the physical modification can be produced by simply adding a surfactant to the lignocellulosic nanoparticles aqueous suspension previous to the freeze-drying process [30, 31]. From a technological point of view, the use of a surfactant is an easily and economically feasible approach to scale up from the lab level to the industrial sector. For food packaging, the surfactant used should be permitted for food contact applications, such as the case of hexadecyltrimethylammonium bromide (CTAB), which has been already used to improve the dispersion of nanoparticles

into the polymeric matrix in food packaging [34]. In fact, Capron *et al.* [35] showed that CTAB enabled a simple, fast, and efficient method for improving the nanocellulose dispersion by reducing the interfacial tension of nanocellulose and thus promoting the repulsion among the nanoparticles.

This work proposes the use of sodium caseinate (SC) protein as the internal layer for two recycled PLA outer layers in a tri-layer packaging system RPLA-SC-RPLA. SC was plasticized with glycerol in 35 wt% on the basis of previous works [17, 36]. Additionally, with the aim to also valorize PLA waste, the PLA layers' formulations were based on recycled PLA, which was obtained by subjecting PLA to an accelerated aging process based on photochemical, thermal, and hygrothermal aging steps, followed by a demanding washing step to pretend the washing process utilized on an industrial recycling scale, following a simulated recycling process previously optimized [37]. To provide the inner layer with an antioxidant functionality, lignocellulosic nanoparticles, extracted from yerba mate waste through a simple aqueous extraction procedure [24], were used as a suitable approach for valorizing this waste in the framework of a circular bioeconomy concept. The YMNs dispersion into the recycled PLA matrix was improved by means of the use of CTAB surfactant. The recycled PLA films (RPLA), RPLA-YMNs nanocomposite films, as well as sodium caseinate films were obtained by solvent casting method. The final tri-layer systems were obtained by compression molding. Then, the structural properties, thermal stability, mechanical performance, and barrier properties (against water vapor and oxygen) of each polymeric film layer as well as of the tri-layer systems were assessed. The antioxidant ability provided by YMNs was studied in a fatty food simulant to get information regarding the possibility of using these multilayer systems as active packaging formulations. Finally, disintegration under composting conditions was studied at a laboratory-scale level as a sustainable end-life option for such materials.

2. Experimental section
2.1. Materials
Poly(lactic acid) (PLA, IngeoTM 2003D), with a density of 1.24 g/cm^3 and a melt flow index of 6 g/10 min (210 °C, 2.16 kg) was provided by NatureWorks (Minnetonka, Minnesota, USA). Sodium caseinate (SC) powder was kindly provided by Ferrer

Alimentación S.A. (Barcelona, Spain). The yerba mate (*Ilex paraguariensis*) waste was collected in our laboratory afterward the drinking of yerba mate infusion. Glycerol (99.5% purity), Cetyltrimethylammonium bromide (CTAB), chloroform (CL, 99.6% purity, boiling point 60 °C), and 2,2-diphenyl-1-picrylhydrazyl (DPPH) 95% free radical were provided by Sigma Aldrich (Madrid, Spain).

2.2. PLA recycling process

Mechanical recycling of PLA was simulated using the process reported by Beltrán *et al.* [37], which is summarized in Figure 1. PLA pellets were dried before processing at 85 °C, under vacuum for 2 h, and further processed by means of melt extrusion process using a Rondol Microlab twin-screw extruder (Rondol, Nancy, France). The temperature profile from hopper to die was: 125–160–190–190–180 °C. The extrusion was carried out at 60 rpm. The obtained material was then pelletized and further compression molded into films with about 200±20 µm in thickness, using an IQAP-LAP hot plate press (IQAP Masterbatch Group S.L., Barcelona, Spain) at 190 °C, for 4 min without pressure, followed by 2 minutes under 200 kg/cm² pressure and 5 minutes, under pressure, between cooling plates. The obtained films were then submitted to an accelerated aging procedure, including (i) 40 h of photochemical degradation in an ATLAS UV-CON chamber (ATLAS, Mount Prospect, Illinois, USA), which is equipped with eight F40 UVB lamps; (ii) 480 h of thermal degradation conducted by putting the samples in a convection oven at 50 °C (P-Selecta, Barcelona, Spain) and (iii) 240 h of hydrolytic degradation at 30 °C in

deionized water. After the aging process, the samples were energetically washed in an aqueous solution of NaOH (1.0 wt%) (Panreac, Barcelona, Spain) and Triton X-100 (0.3 wt%) (Alfa Aesar, Kandel, Germany), at 85 °C for 15 minutes. The washed material was then shredded and reprocessed by melt extrusion and compression molding, using the same conditions stated above.

2.3. Extraction of Yerba mate nanoparticles (YMNs)

The extraction of the yerba mate nanoparticles (YMNs) from yerba mate waste was performed following the recipe previously developed by Arrieta *et al.* [24], with slight modifications. In brief, the obtained yerba mate waste from the 'mate' infusion was dried in a sun exposure window for a week and further completely dried in a vacuum oven at 40 °C for 24 h. Then, 6 g of the dry yerba mate residue were put in a flask with 200 mL of distilled water and were heated under continuous stirring at reflux up to 100 °C. The solid residue was detached by filtration, and the yerba mate extract was filtered off again under vacuum (Whatman Grade 41 filter paper). The YMNs were physically modified by adding a cationic surfactant, CTAB surfactant, to the yerba mate extract suspension in 1/1 (w/w) and stirred overnight [38]. Then, the yerba mate extract was frozen and then freeze-dried to obtain the YMNs powder. The procedure of YMNs extraction is schematically represented in Figure 2.

2.4. Film preparation

Sodium caseinate films were developed following a previously developed recipe [17, 36]. In brief, sodium
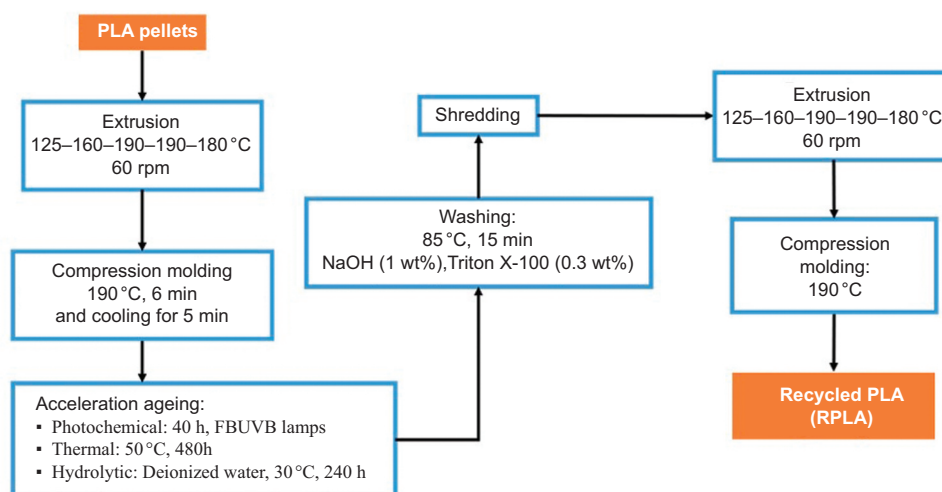

Figure 1. Schematic representation of the simulated recycling process of PLA.
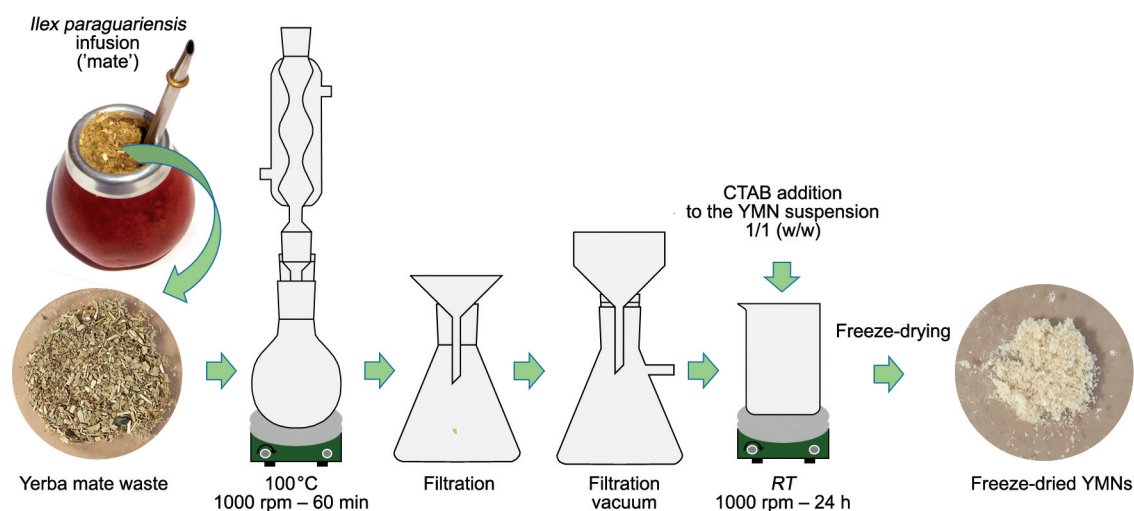
Figure 2. Schematic representation of YMNs extraction from yerba mate waste.

caseinate was dissolved in deionized water under constant stirring at 1000 rpm, to get casting solutions of 5 (w/w) concentration. Glycerol at a concentration of 35 wt% dry basis was added as a plasticizer to the polymeric solution. Such a concentration of glycerol was selected to plasticize the sodium caseinate guaranteeing that the films can be handled without breaking, as happens when lower plasticizer contents are used [36]. The caseinate-glycerol solutions were ultrasonic degasified at room temperature to eliminate foams and air bubbles, and then 30 ml of these solutions were cast into 15 cm diameter polyethylene Petri dishes, then the water was allowed to evaporate in an oven at 40±2 °C for 48 h, and finally, the plasticized sodium caseinate films were obtained (SC).

For the preparation of PLA films and PLA-YMNs nanocomposites, RPLA (0.6 g) was dissolved in 60 ml of chloroform adding 1 or 3 wt% of YMNs to obtain RPLA-YMN1 and RPLA-YMN3, respectively. The film formulations were obtained after solvent evaporation in 10 cm diameter glass mold at room temperature.

The tri-layer systems were prepared by successfully compression-molding the previously developed monolayer systems in a RPLA/SC/RPLA or RPLA/SC/RPLA-YMN structure. The tri-layers were compression-molded and assembled in a hot press at 130 °C in an IQAP-LAP hot plate press (IQAP Masterbatch Group S.L., Barcelona, Spain) for 2 min without pressure and then 5 min at 200 kg/cm², and cooled down to room temperature in 5 min at 200 kg/cm². Three tri-layer film formulations were

obtained and labeled as: RPLA/SC/RPLA, RPLA/SC/RPLA-YMN1, and RPLA/SC/RPLA-YMN3.

2.5. Characterization techniques
2.5.1. Characterization of YMNs

Attenuated total reflection-Fourier transform infrared (ATR-FTIR) spectroscopy was used to conduct chemical analysis of the yerba mate nanoparticles extraction and modification with CTAB surfactant. A Nicolet iS10 spectrometer (Thermo Fisher Scientific, Waltham, Massachusetts, USA), equipped with a Smart iTR Attenuated Total Reflectance (ATR) accessory controlled by OMNIC Software (9.9.473 version) was used to record the FTIR spectra. The resolution used was 4 cm⁻¹, and 16 spectra were recorded for each sample between 4000 and 550 cm⁻¹.

The particle size of the YMNs with and without surfactant after the freeze-drying process was measured at 20 °C with a dynamic light scattering (DLS) analyzer (Zetasizer Nano series ZS, Malvern Instrument Ltd., U.K.) equipped with a He-Ne laser beam at 658 nm and with a detection angle of 173°. YMNs were dispersed in water (1 mg/ml) for 5 min in an ultrasonic bath, and the reported particle size measurements were the average value of at least six consecutive runs.

YMNs were observed by Transmission Electron Microscopy (TEM, JEOL JEM-1010) operating at 100 kV. YMNs powder (1 mg) was suspended in 2 ml of water, and one droplet of YMNs suspension was deposited on carbon-coated copper grids and

dried at room temperature for 20 min previously to be observed.

2.5.2. Characterization of monolayer and tri-layer films

The absorption spectra in the 800 200 nm region of RPLA, SC as well as tri-layer films were investigated by means of a Varian Cary 1E UV-Vis spectrophotometer (Varian, Palo Alto, California, USA) with an integrating sphere. The overall transmittance in the visible region was then calculated according to the ISO 13468 standard [39]. The measurements were performed using a scanning speed of 400 nm/min.

The structure of the tri-layer films was analyzed by Confocal Raman microspectroscopy, using a Thermo Scientific™ DXR3 spectrometer (Thermo Fisher Scientific, Waltham, MA, USA) with a CCD camera coupled to an Olympus confocal microscope. The cross-section images of the films probed the obtainment of homogeneous tri-layer structures. Raman spectra were acquired in the 3400–100 cm^{-1} region. The Raman scattering was excited using a diode laser at a wavelength of 780 nm. All spectra were collected by coadding 64 scans, with an acquisition time of 10 s. The pinhole diameter was 50 µm. The laser beam was focused on the tri-layer formulations with a microscope objective. The spectra of each layer and the interfacial regions were acquired. In these conditions, the resolution of the spectral shift was about 2.5 cm^{-1}.

Thermogravimetric analysis of the film samples was performed in a TGA2050 thermobalance (TA Instruments, New Castle, Delaware, USA). Samples of about 5–10 mg were heated from 40 to 800 °C, at 10 °C/min under a nitrogen atmosphere.

DSC experiments were conducted in a Q20 calorimeter (TA Instruments, New Castle, Delaware, USA) under a nitrogen atmosphere (50 ml/min). Tri-layer film samples of about 5 mg were put in standard aluminum pans and heated from 30 to 180 °C at 5 °C/min. Tensile tests were performed at room temperature by means of a Shimadzu AGS-X 100N tensile testing machine (Shimadzu Corporation, Kyoto, Japan) equipped with a 100 N load cell, according to ASTM D882-01 Standard. Tensile tests were performed in rectangular strips (5×50 mm^2), initial grip separation 30 mm, and crosshead speed 10 mm/min. Tensile strength (TS), elastic modulus (E), and average percentage deformation at break (ε_B [%]) were obtained from the resulting stress-strain curves as the

average of at least five determinations from three films of each formulation.

Oxygen permeability analyses were carried out at 30 °C in a homemade permeation cell [40] at a gas pressure of 1 kPa.

The water vapor transmission rate (WVTR) measurements of the tri-layer formulations were determined by gravimetry according to the ISO 2528 standard [41]. Permeability cups were filled with 2 g of dry silica gel, sealed with each tri-layer film, and weighted. The permeability cups were exposed to a saturated KNO$_3$ solution in a desiccator at 23±1 °C (approximately 90% RH). Then, the permeability cups were reweighed each hour during 6 h, and the WVTR [g/(day·cm^2)] was calculated from Equation (1):

$$WVTR = \frac{240 \cdot m_t - m_0}{A \cdot t} \tag{1}$$

where m_t is the mass of the permeability cup at time t, m_0 is the mass of the permeability cup at the beginning of the assay, and A is the exposed area of the tri-layer film. Then the water vapor permeability (WVP) was calculated according to Equation (2):

$$WVP = \frac{WVTR}{S \cdot (R_1 - R_2)} \cdot d \tag{2}$$

where S is the saturation vapor pressure of water at 23 °C, R_1 and R_2 are the relative humidity in the desiccator and inside the cup, respectively, and d is the thickness of the film.

Due to the fact that the tri-layer films developed here are intended for fatty food packaging applications, migration tests were carried out in triplicate by the development of YMN-specific migration tests in food simulant D1 (solutions of 50% v/v ethanol). Circular samples of 2.2 cm diameter were put in a glass vial cap, and the vials were filled to 5 mm from the edge. The filled vials were placed upside down in an oven and were kept at 40 °C for 10 days. The antioxidant activity of the released YMNs was measured by means of the DPPH-method by measuring the maximum absorbance of DPPH radical in the presence of the released YMNs in the food simulant D1 after 10 days [13] by means of a Varian Cary 1E UV-Vis spectrophotometer (Varian, Palo Alto, California, USA) which is equipped with an integrating sphere. The UV-vis measurements were recorded at 518 nm and using a scanning speed of 400 nm/min. The antioxidant activity was determined according to Equation (3):

$$I\,[\%] = \frac{A_{\text{control}} - A_{\text{sample}}}{A_{\text{control}}} \cdot 100 \qquad (3)$$

where $I\,[\%]$ is the percentage of inhibition, A_{control} is the absorbance at 518 nm of DPPH in ethanolic solution and A_{sample} is the absorbance at 518 nm of DPPH after 15 min maintained at darkness in contact with the ethanolic solution (food simulant D1) containing the released antioxidant compounds. The antioxidant properties of the films were determined in triplicate, and the results of the % of inhibition were expressed as the equivalent of gallic acid (GA) concentration [mg/kg] by using a calibrated curve of gallic acid concentration *versus I* [%].

The tri-layer films were then fully disintegrated under composting conditions at a laboratory-scale level. The composting test was performed following the ISO 20200 standard [42]. Film samples of 1.5×1.5 cm were buried at 4–6 cm deep in a solid synthetic waste contained in perforated plastic reactors. To maintain the tri-layer film samples in direct contact with the compost medium and to allow the removal of disintegrated film samples from the compost for further analysis, each sample was kept in a textile mesh [38]. The solid synthetic waste was prepared by 10 wt% of mature compost (Compo Group, Barcelona, Spain), 40 wt% of sawdust (Productos Adrian, Valencia, Spain), 30 wt% of dwarf rabbit food (Vitakraft, Bremen, Germany), 10 wt% of starch (Unilever Spain, Barcelona, Spain), 5 wt% of sugar (Azucarera, Madrid, Spain), 4 wt% of corn oil (Koipe, Córdoba, Spain) and 1 wt% of urea (Quimipur, Madrid, Spain). Then, provide the compost medium with water, 50 wt% water was incorporated into the solid synthetic waste. The reactors containing the buried tri-layer films were kept in an oven (Memmert GmbH, Schwabach, Germany) under aerobic conditions at 58 °C. Disintegrated tri-layer film samples were removed from the compost medium at 4, 7, 11, and 17 days. The disintegrated samples were reweighted after each extraction in a QUINTIX125D-1S analytical balance (Sartorius, Gotinga, Germany) to calculate the degree of disintegrability following Equation (4):

$$\textit{Disintegration degree}\,[\%] = \frac{w_0 - w_t}{w_0} \cdot 100 \qquad (4)$$

In which w_0 is the initial weight of the tri-layer film sample before composting test and w_t is the weight of the tri-layer specimens after t (4, 7, 14, and 17) days exposed to the composting medium. Then, the recovered tri-layer pieces were dried at 40 °C under vacuum in an oven and stored under vacuum for characterization. Moreover, photographs of the tri-layer film samples were taken before and during the composting test to have a qualitative check of the materials' degree of physical disintegration in the compost medium as a function of time. Photographs of the compost soil were also taken, while the pH was measured with a Hach SesION™ + pH meter (Hach Company, Loveland, Colorado, USA).

Significance in mechanical properties, as well as antioxidant migration studies, was calculated using one-way analysis of variance (ANOVA) with Origin Pro 8 software SRO v8.0724 (OriginLab Corporation, Northampton, MA, USA). To identify which groups were significantly different from other groups means comparisons were made by performing a Tuckey's test with a 95% confidence interval, and the reported *p*-values were considered statistically significant at $p < 0.05$.

3. Results and discussion
3.1. Yerba mate nanoparticles characterization

The lignocellulosic nanoparticles used here for the development of RPLA-based nanocomposites were obtained from yerba mate waste, as it was described in previous work [24]. To corroborate the success of the complete removal of hemicellulose component from the yerba mate waste, the yerba mate waste, as well as the obtained YMNs were characterized by ATR-FTIR. The band around 1730 cm⁻¹ belongs to the acetyl and ester groups in hemicelluloses [43]. As can be seen in Figure 3a, the hemicellulose component was initially present in the yerba mate solid waste, while it disappeared in YMNs, confirming the successful obtainment of lignocellulose nanoparticles [24]. Moreover, the C–H stretching vibration band corresponding to alkyl groups in aliphatic bonds of hemicellulose, lignin, and cellulose, appeared around 2850 cm⁻¹ in yerba mate waste, and it is reduced in YMNs as it has been already observed during YMNs extraction process [24, 29]. The incorporation of CTAB to the YMNs showed the appearance of two strong bands at 2900 and 2850 cm⁻¹ in Figure 3b, corresponding to the antisymmetric and symmetric CH₂ stretches [44, 45]. The presence of the band at 1270 cm⁻¹ (associated with the aromatic skeletal vibrations), the presence of the band at 1155 cm⁻¹ associated with C–H out-of-plane as well
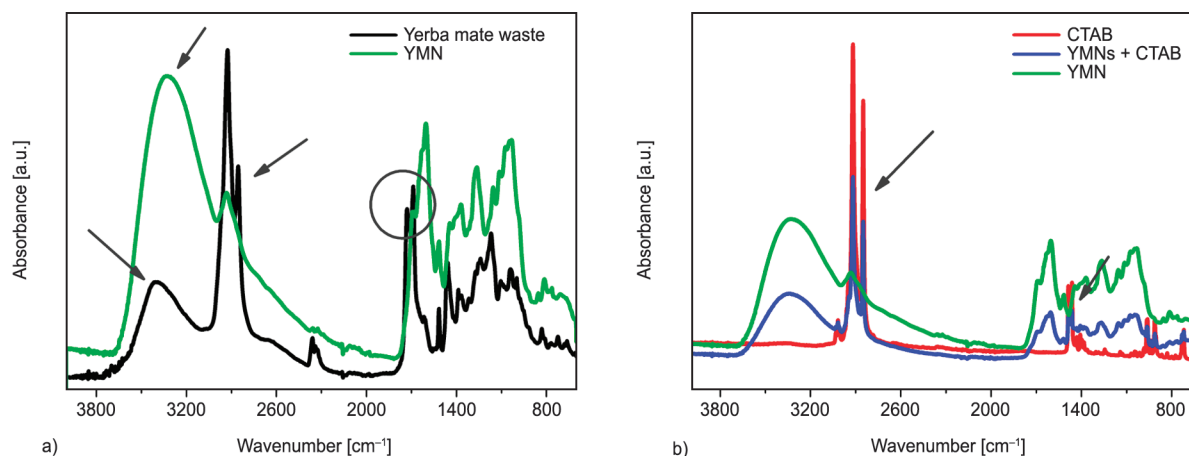
Figure 3. FTIR spectra of: a) erba mate waste and yerba mate nanoparticles without CTAB and b) CTAB, yerba mate nanoparticles without CTAB, and yerba mate nanoparticles with CTAB.

as the presence of the band at 1112 cm^{-1} and the typical aromatic C–H bending in-plane, are suggesting that lignin remains present in YMNs and, thus, indicating the lignocellulosic nature of yerba mate nanoparticles [24].

It is widely known that the freeze-drying process produces the agglomeration of lignocellulosic nanoparticles. Thus, in the present work, with the aim of obtaining a stable suspension of YMNs, CTAB surfactant was added to physically functionalize the surface of lignocellulosic nanoparticles. In Figure 4a are shown the hydrodynamic size of freeze-dried lignocelullosic nanoparticles with and without the addition of surfactant. In the case of YMNs without surfactant, there is a major peak from 20 to 170 nm centered between 40 and 60 nm, as well as another peak between 170 to 500 nm, probably due to the formation of lignocellulosic nanoparticles agglomerations [24]. In the case of surfactant added lignocellulosic nanoparticles, although there was not a particle size reduction, there was a narrowing of the nanoparticles' main peak, which was between 20 and 90 nm, and a small shoulder of the previously mentioned agglomerated nanoparticles. The surfactant did not influence the sizes of the nanoparticles because it has a small short-chain [44], but it seems that it allowed better dispersion of the lignocellulosic nanoparticles. It is known that the hydrophilic part of the surfactant can be adsorbed on the surface of lignocellulosic nanoparticles, while the hydrophobic part is able to provide a nonpolar surface that lowers the surface tension of such nanoparticles favoring the dispersion with nonpolar polymers [30, 31]. In Figure 4b is represented the proposed interaction mechanism of lignocellulosic nanoparticles by means

of hydrogen bonding interactions and the lignocellulosic nanoparticles with the presence of surfactant, which the surfactant avoids or at least reduce the hydrogen bonding interactions between lignocellulosic nanoparticles hydroxyl groups. However, it should be taken into account that the DLS technique is designed to calculate the hydrodynamic diameter of spherical particles, therefore, TEM observations were also conducted. In Figure 4c is shown a TEM image of freeze-dried yerba mate nanoparticles prior to the addition of CTAB surfactant. It is clearly seen that the nanoparticles are agglomerated in accordance with previous works [11, 29]. In fact, from the zoom image of Figure 4c is evident that several nanoparticles are interacting, forming agglomerates. Meanwhile, from the TEM image of the freeze-dried YMNs physically modified with CTAB surfactant Figure 4d, it can be observed that YMNs exhibit dimensions ranging from 50 to 100 nm in length, in good agreement with YMNs suspensions before the freeze-dried process [24, 29]. Although the nanoparticles are somewhat accumulated, it can be seen from the zoom image of Figure 4d that lignocellulosic nanoparticles can be isolated, and it is clear that they show the typical shape of a whisker. Therefore, it can be concluded that the surface modification with a surfactant does not affect the morphology or the sizes of the nanoparticles but can reduce the interaction among them, limiting the agglomeration. Similar findings have been already observed by de Souza *et al.* [44] in cellulose nanoparticles modified with anionic surfactants.

3.2. Film characterization
Transparent SC and RPLA monolayer films were obtained, and the tri-layer formulations successfully
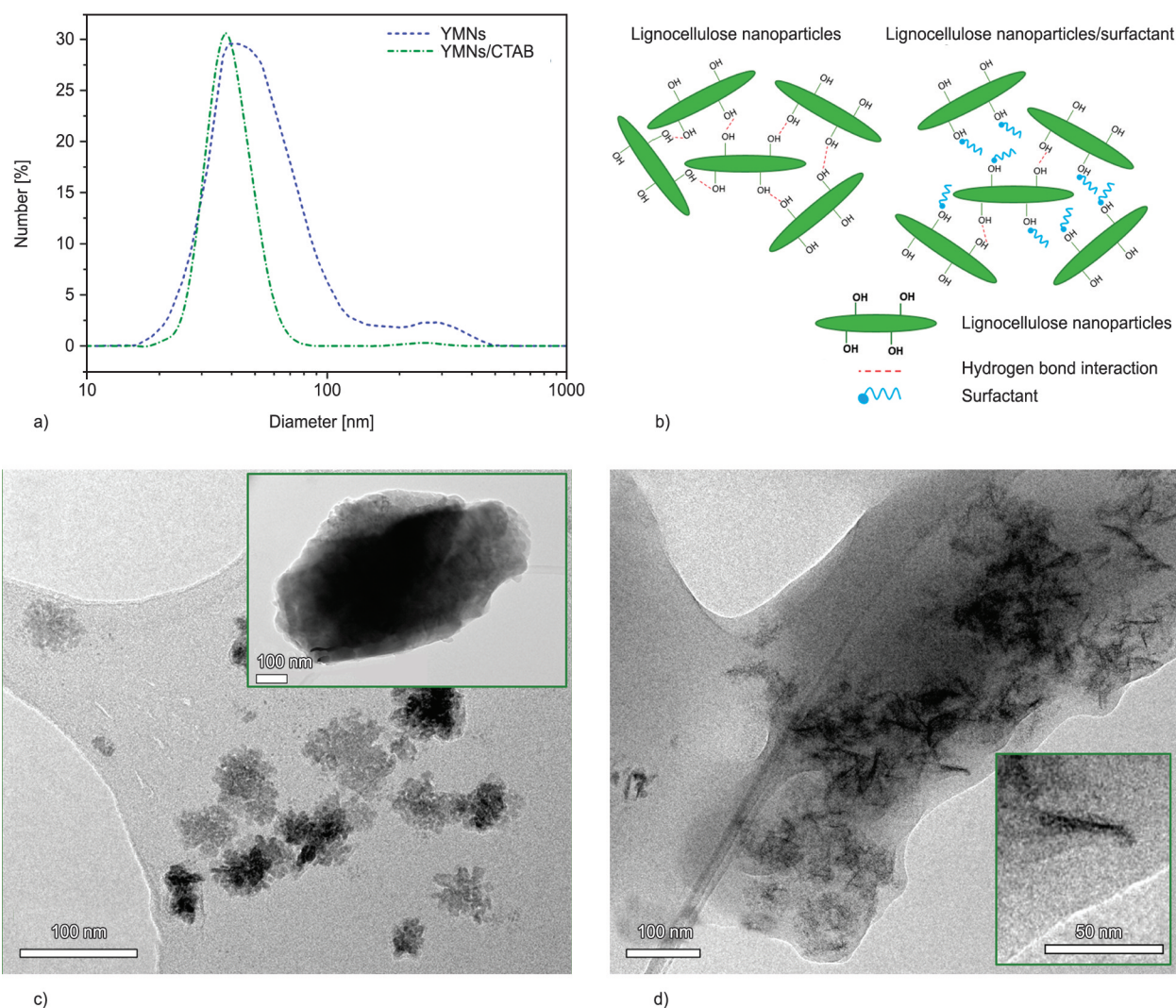
Figure 4. a) DLS measurements of YMNs with and without CTAB incorporation before the freeze-dried process, b) schematic representation of hydrogen bonding interaction between lignocellulosic nanoparticles with and without the presence of a surfactant, c) TEM image of freeze-dried YMNs without surfactant and d) TEM image of freeze-dried YMNs modified with CTAB surfactant.

maintained transparency (Figure 5a), even in the presence of YMNs. It seems that the good dispersion of YMNs as well as the low thickness of the obtained materials allowed to obtain transparent films. These findings were corroborated by means of UV-vis spectrometry (Figure 5b). The spectra show that RPLA films are highly transparent and very similar to that of virgin PLA in the visible region. However, in the UV region (250–400 nm), the recycled polymer showed different behavior, as it presents lower UV light transmission than virgin PLA, with the appearance of a small absorption peak at 277 nm. This peak is correlated with the presence of chain-end carboxyl groups during the mechanical recycling process [46, 47]. In the case of the YMNs-reinforced nanocomposite films, it should be mentioned that

this UV region is also overlapped with absorption peaks of different polyphenols present in the YMNs (*i.e.*, chlorogenic acid, caffeic acid, and rutin) [24]. Concerning the transparency of the tri-layer structures (Figure 5c), it was observed that the high transmittance of RPLA/SC/RPLA was practically maintained in the RPLA/SC/RPLA-YMN formulations although a slight reduction in the transmittance was observed along with the visible spectra with increasing content of YMNs. The maintenance of good transparency of PLA-based nanocomposite films reinforced with lignocellulosic nanoparticles has been ascribed to the homogeneous dispersion of nanoparticles into the PLA matrix, which could be substantially improved by the addition of surfactants to modify lignocellulosic nanoparticles surface tension [31, 38].
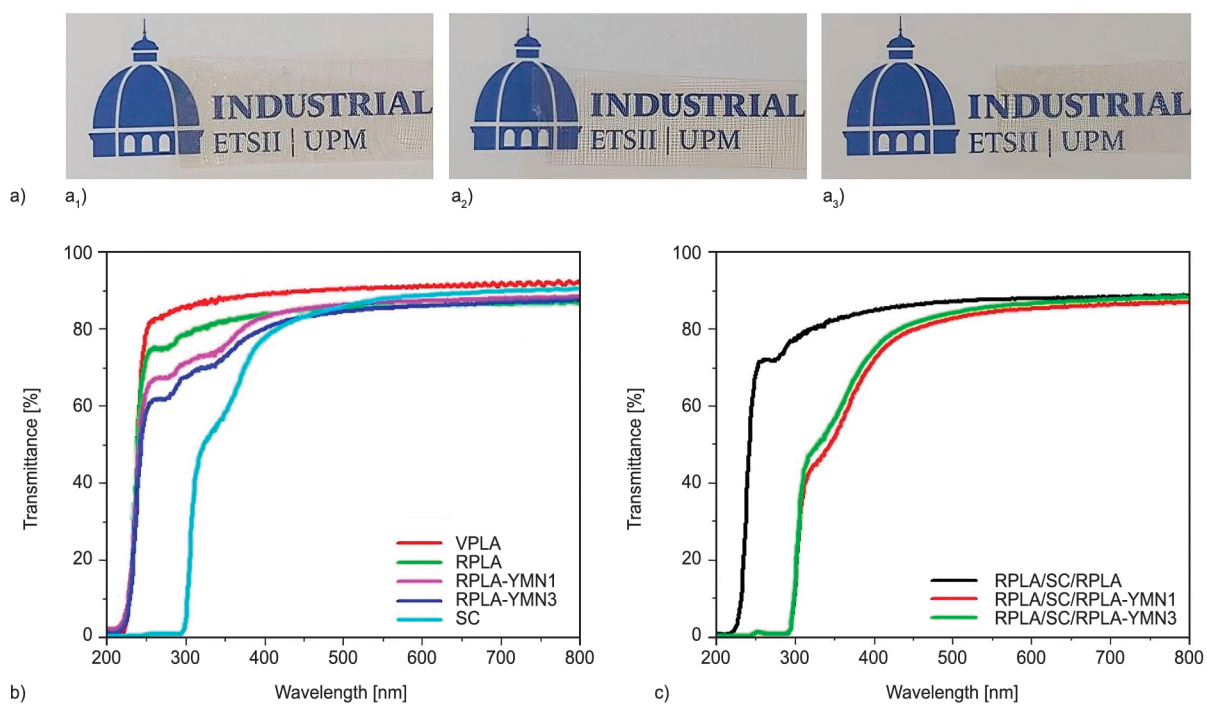
Figure 5. a) Visual appearance of tri-layer films: a₁) RPLA/SC/RPLA, a₂) RPLA/SC/RPLA-YMN1, a₃) RPLA/SC/RPLA-YMN3. b) UV-vis spectra of monolayer films, and c) UV-vis spectra of tri-layer films.

The morphological aspects of the tri-layer structure were studied by confocal microscopy, mainly to corroborate the success of the developed procedure to produce the tri-layer structure (Figure 6).

From the cross-section of the tri-layer RPLA/SC/RPLA films, each layer can be clearly distinguished. Meanwhile, they showed good adhesion between them, as can be seen from the absence of phase separation between SC and PLA-based polymeric layers. The RPLA external layers were very thin (thickness of about 10–30 µm), while the sodium caseinate internal layer resulted thicker and, thus, the final thickness was governed by the SC layer

leading to final tri-layer films with a thickness between 70 and 115 µm.

Thermal stability plays a very important role in the processing of plastics since it is a limiting factor for choosing the processing temperature of the materials as well as their service temperature. The thermal stability of the different monolayer and tri-layer films was studied by means of TGA, and the main results are summarized in Figure 7.

Figure 7a shows the dynamic TGA curve and the derivative curve of the plasticized caseinate film. The analyzed sample showed several weight loss regions. Such behavior is similar to that reported in other
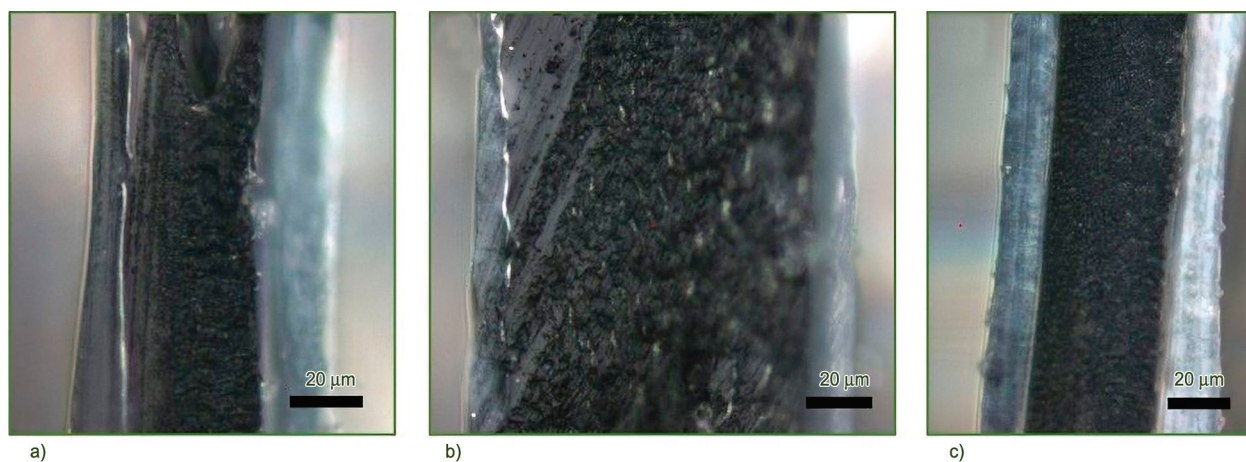

Figure 6. Confocal optical microscope observations of the cross-section of a) RPLA/SC/RPLA, b) RPLA/SC/RPLA-YMN1, and c) RPLA/SC/RPLA-YMN3 (100×).
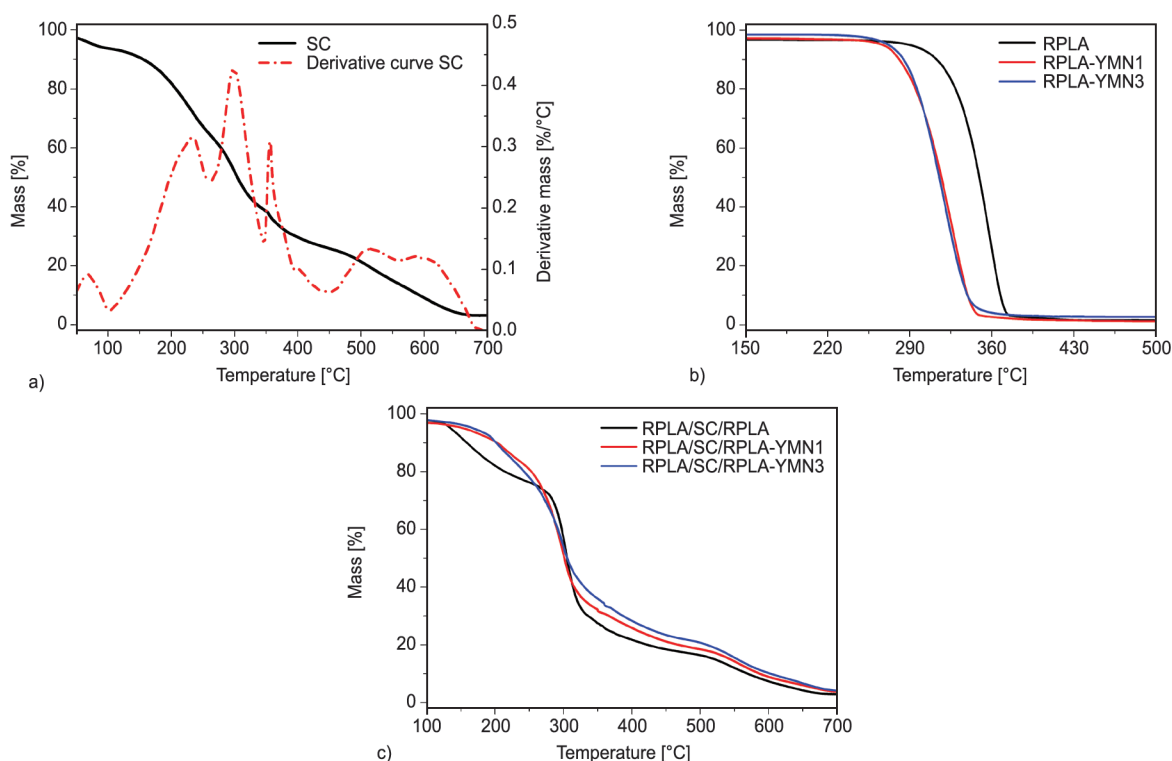
Figure 7. TGA curves of a) sodium caseinate monolayer films, b) PLAR monolayer films, and c) tri-layer films.

works, such as Pereda *et al.* [16] and Arrieta *et al.* [36]. The first region, located below 100 °C, corresponds to the evaporation of water. The second region, located between 100 and 240 °C, corresponds to the loss of the glycerol plasticizer, and the third region, above 300 °C, is assigned to the degradation of the proteins of the sodium caseinate matrix. Regarding the thermal stability of PLAR and PLAR nanocomposites, Figure 7b shows that all PLA monolayer films presented only one degradation process. It can also be seen that the addition of the YMNs led to a decrease of the thermal stability of the PLA matrix. A similar result was reported by Beltrán *et al.* [29] in recycled PLA-YMN nanocomposites prepared by melt extrusion. The reduction in the thermal stability was attributed to the lower thermal stability of the YMNs, which reduced the overall thermal stability of the materials. Figure 7c shows the dynamic TGA curve of the tri-layer systems. It can be seen that the samples show the decomposition processes of both the sodium caseinate and PLA layers. However, it is worth noting that the incorporation of YMNs in one of the layers led to a slight increase in the thermal stability of the samples. This result suggests that the YMNs have a protective effect on the sodium caseinate layer due to their antioxidant properties ascribed to the high content of polyphenols [24]. The improvement of thermal stability can also be ascribed to the well-dispersed YMNs in the PLAR due to the CTAB surfactant presence. The improvement of lignocellulose nanoparticles' thermal stability due to physical or chemical modifications has already been observed [30–32].

The thermal transitions of the different materials were analyzed by means of DSC analysis. Figure 8 shows the first heating scan of the single layers (Figure 8a) and the tri-layer samples (Figure 8b). Figure 8a shows that the sodium caseinate layer presents a wide endothermic peak around 70 °C, which can be related to the evaporation of water present in the caseinate layer. Regarding the behavior of the recycled PLA films, it can be seen that all samples show the characteristic thermal behavior of recycled PLA: (i) a glass transition below 60 °C; (ii) an exothermic peak above 100 °C, corresponding to the cold crystallization; and (iii) an endothermic double melting peak [12, 37]. The presence of this double melting peak can be related to a melt recrystallization mechanism, as was pointed out by Di Lorenzo [48], in which the less perfect crystals melt at lower temperatures, rearrange themselves and melt again at higher temperatures. It is worth noting that both nanocomposites show higher glass transition and cold crystallization temperatures. This increase suggests that the presence of lignocellulosic nanoparticles limits the mobility of the PLA molecular segments, thus making difficult
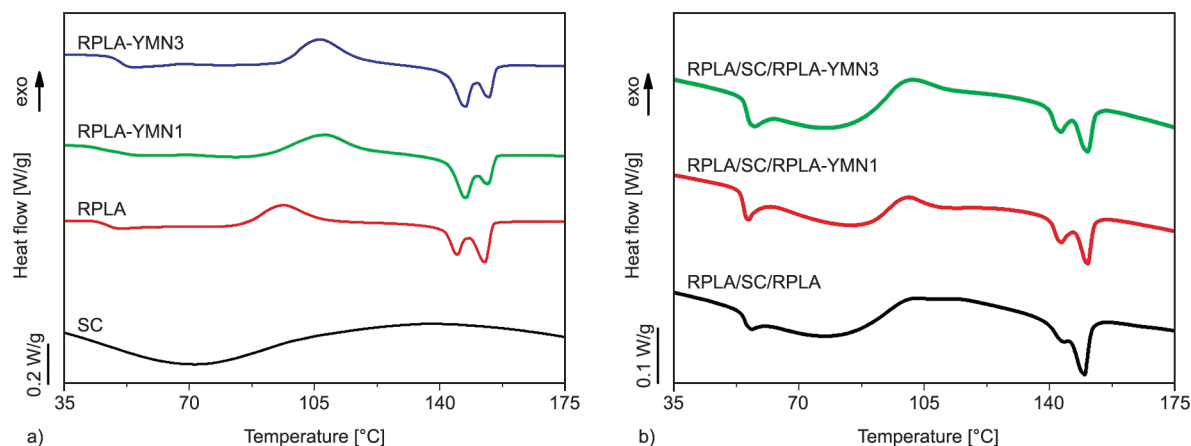
Figure 8. DSC heating scans of a) single layer and b) tri-layer sample.

the glass transition and the crystallization of the polymer matrix. Similar results have been reported by Gordobil *et al.* [49] and Bužarovska *et al.* [50], in PLA-based lignin composites.

Figure 8b shows the first heating scans of the tri-layer systems. It can be seen that the behavior of the different samples is very similar. All of them show the characteristic thermal behavior of PLA, although the broad endothermic peak at 70 °C of the sodium caseinate layer is noticeable in the three multilayer systems. Furthermore, it is worth noting that the enthalpy values for cold crystallization and melting are lower. This decrease can be attributed to the PLA layers being a small part of the sample since confocal microscopy analysis showed that the sodium caseinate layer was the predominant layer in the samples. Therefore, the inclusion of a sodium caseinate layer

has only a limited effect on the thermal transitions of the materials since it does not affect the crystallization nor the melting temperatures of both PLA layers in contact.

Raman microspectroscopy is widely used for the characterization of multilayer polymer structures [51]. Raman spectra allow the identification of the polymer present in each layer, and the coupling to optical microscopy adds the capability of measuring the width of the different layers [52]. Moreover, as occurs in all vibrational spectroscopies, Raman spectra are very sensitive to the local molecular environment, which gives useful information on the molecular structure of the polymers [53]. Figure 9 shows the Raman spectra of a tri-layer structure representative of the materials studied in this work, formed by the outer layers of RPLA and RPLA nanocomposites
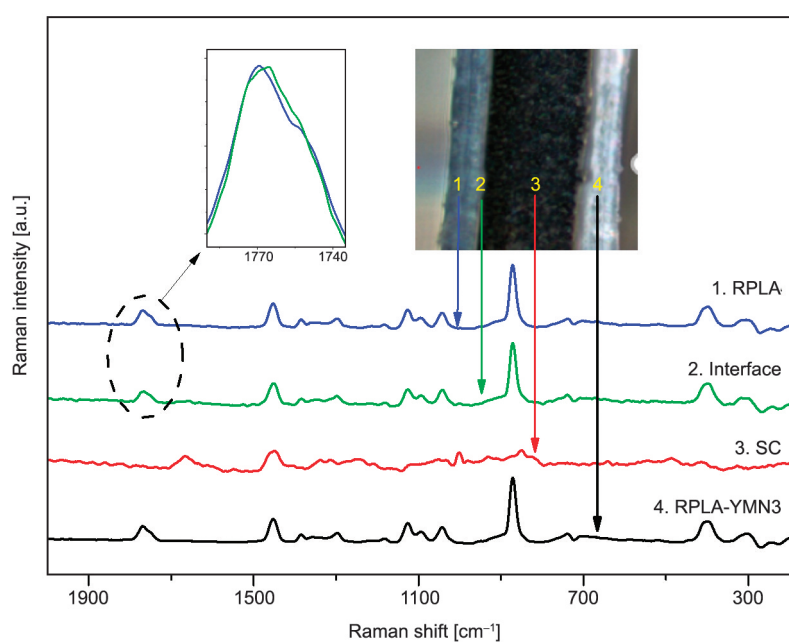

Figure 9. Raman spectra of RPLA/SC/RPLA-YNM3 tri-layer film with the corresponding confocal microscopy image (50×).

reinforced with 3 wt% of yerba mate nanoparticles (RPLA/SC/RPLA-YMN3). The Raman spectra were measured at the points indicated in the tri-layer image inserted in the figure. The spectrum of the RPLA layer shows the characteristic bands of the Raman spectrum of this polymer, such as those that appear at 1770, 1454, 870, and 410 cm^{-1}, which can be assigned to C=O stretching, CH$_3$ bending, C–COO stretching, and C=O deformation, respectively, according to the bibliography [54]. Spectrum 3, recorded in the intermediate layer, shows the characteristic bands of the Raman spectrum of sodium caseinate, especially those that appear at 1667 cm^{-1} (amide I), 1452 cm^{-1} (amide II) [55], and 1004 cm^{-1}, which has been assigned to the presence of phenylalanine [55]. Spectrum 4 corresponds to the layer of RPLA with yerba mate nanoparticles. It is a spectrum very similar to that of RPLA since the bands corresponding to nanoparticles are very weak due to the low amount of nanoparticles.

One of the main advantages of Raman confocal microspectroscopy is the ability to measure in very small areas of the material, with diameters of about 3 μm. This ability has been used to compare the RPLA spectrum measured in bulk with the spectrum measured at the interfacial region between the different layers in order to study the existing chemical interactions. Thus, Figure 9 also shows the Raman spectrum measured at the interface between the RPLA and sodium caseinate layers (see no. 2 spectrum). This spectrum shows the characteristic bands of both substances, although the bands corresponding to PLA are more intense. It is important to note that the spectra of RPLA measured in the interface and in bulk are slightly different, as shown in the inset of Figure 9. In this inset, a very slight shift towards lower wavenumbers (lower energies) can be observed in the C=O stretching band measured at the interface, which could correspond to the formation of hydrogen bonds between RPLA and sodium caseinate. It is well known that hydrogen bonding leads to shifts to lower frequencies and broadening of the carbonyl stretch band [53]. This possible formation of hydrogen bonds is important because it would indicate a good adhesion between RPLA and sodium caseinate layer, which could be used to obtain multilayer structures with good properties. The existence of hydrogen bonding interactions has already been suggested for multilayer films based on PLA, and soy protein isolate plasticized with glycerol (SPI-G) [56] or PLA

with gelatin plasticized with glycerol (Ge-G) [14]: PLA/SPI-G/PLA [56] and PLA/Ge-G/PLA [14].

Films for food packaging are required to protect foodstuff from mechanical stress during transport, storage, and conservation. Thus, the mechanical performance of the tri-layer formulations was evaluated by means of tensile test measurements, and the results in terms of the tensile strength (*TS*), elastic modulus (*E*), and elongation at break (ε$_B$) are summarized in Table 1, and the tensile curves are represented in Figure 10.

Caseinate-based films are very fragile materials, and this is why sodium caseinate matrix requires plasticization [16, 36]. In this work, SC was plasticized with glycerol, and the materials showed flexibility with a consequent reduction in the *TS* and *E* of sodium caseinate proteins [36]. The low mechanical strength of caseinate films is one of the reasons that limit their use in food packaging applications, and it is expected that the PLA layer governs the bi-layer structure. Regarding the PLA-based monolayer films,

Table 1. Tensile test properties of mono-layer and tri-layer films **[%]**.

	E [MPa]	*TS* [MPa]	ε$_B$ [%]
SC	25.0±0.8[a]	2.5±0.5[a]	135.4±12.1[a]
RPLA	1900±100[b]	48.0±3.3[b]	6.4±0.7[b]
RPLA-YMN1	800±50[c]	15.3±2.1[c]	5.4±1.3[b]
RPLA-YMN3	1400±100[d]	24.8±4.4[d]	6.8±1.4[b]
RPLA/SC/RPLA	1000±50[e]	22.8±2.2[d]	7.0±0.4[b]
RPLA/SC/RPLA-YMN1	1100±50[e]	25.1±3.0[d]	5.2±0.8[b]
RPLA/SC/RPLA-YMN3	900±50[c,e]	23.2±2.0[d]	7.8±0.9[b]

[a-e]Different letters within the same column indicate significant differences between the indicated values of the film formulations ($p < 0.05$).
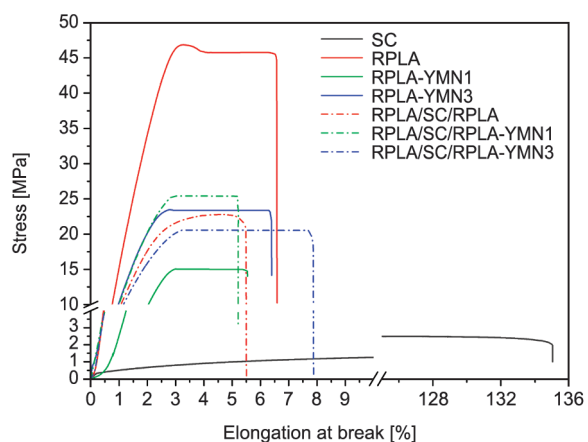

Figure 10. Stress-strain curves of monolayer and tri-layer films.

it was observed that the *TS* and *E* values of the recycled PLA monolayer film (RPLA) were reduced due to the addition of YMNs, while the elongation at break was maintained ($p > 0.05$). When using low amount of YMNs, that is 1 wt%, it seems that, although the modification of YMNs improved their dispersion, YMNs caused local stress concentrations, and then the nanocomposites fail at reduced strain values. Similar findings have already been observed in surfactant-modified cellulose nanocrystals reinforced PLA-based nanocomposites [31]. Nevertheless, it should be highlighted that the *TS* and *E* significantly ($p < 0.05$) increased with an increasing amount of YMNs to 3 wt%, showing the reinforcing ability of such lignocellulosic nanoparticles [24]. In the case of the tri-layer films, the elastic modulus and the elongation at break were controlled by the PLA layer, while the mechanical behavior of the tensile strength was not an average of the individual properties of monolayer films, but intermediate values between RPLA and SC layers were obtained, as frequently occurs in multilayer polymeric films [13, 16]. Kristo *et al*. [19] developed caseinate/pullulan bilayer films as well as caseinate-pullulan blends and observed that the mechanical response of blends depends to a greater extent on the good interaction between both polymeric matrices, while in bilayer systems, no strong stress concentration effect exists near the interface since it is aligned along the tensile direction. Our results are in good agreement with those obtained by Martucci and Ruseckaite [14], who developed tri-layer films

based on two external layers of PLA and an internal layer of glycerol plasticized gelatin (Ge-G). The elastic modulus and the elongation at break of PLA/Ge-G/PLA system were mainly that of the PLA individual layer, and the tensile strength was an intermediate value of both polymers with a higher influence by the PLA layer. They concluded that the mechanical behavior of the tri-layer films did not answer to a simple blending rule and ascribed the obtained results to interactions between polymeric layers, such as hydrogen interactions established at the gelatin/PLA interface [14]. As it was already commented, we also observed some evidence of hydrogen bonding interactions by means of Raman spectroscopy.

Gas barrier properties are very important for materials intended for food packaging applications. One of the key degradation agents in food is oxygen since it takes part in a wide array of undesirable reactions such as enzymatic browning, vitamin loss, lipid oxidation, and microorganism growth [3, 17, 57]. Figure 11a shows the oxygen permeability results for the different samples. It can be seen that the sodium caseinate films showed excellent oxygen barrier properties, as has been previously reported in different studies [17, 57, 58]. In the case of multilayer films, all samples show lower oxygen permeability than the value reported by Rocca-Smith *et al*. [7] for pure PLA ($3.81 \cdot 10^{-12}$ mol·m/(m²·s·Pa)). This considerable improvement of the oxygen barrier properties can be attributed to the presence of the inner sodium caseinate layer. Similar results have been observed by
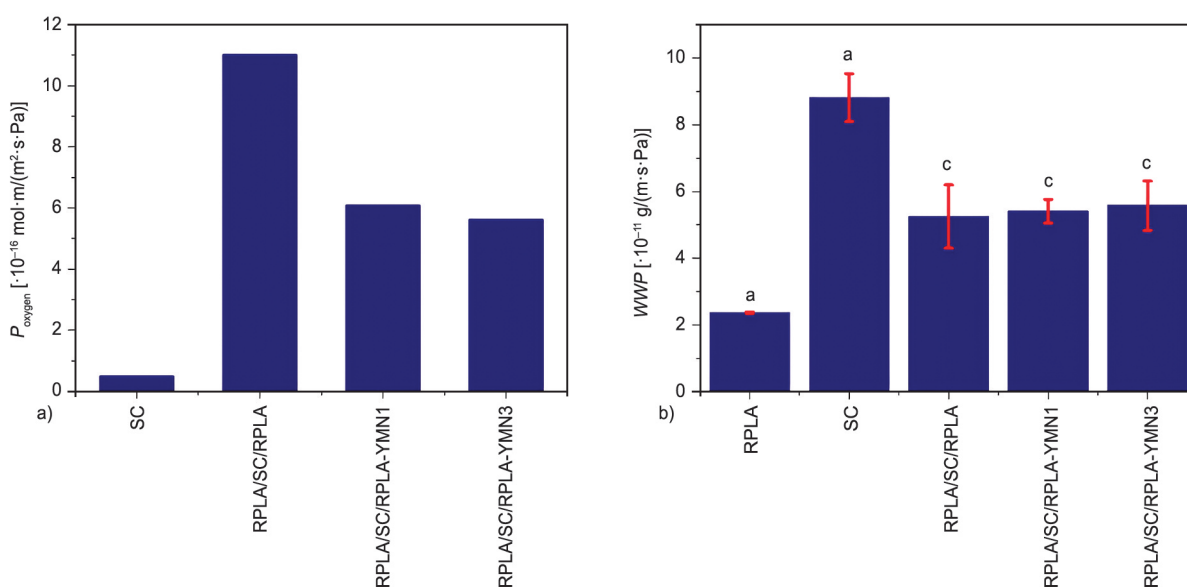

Figure 11. a) Oxygen permeability and b) water vapor permeability of the different samples. [a,c]Different letters on the WVP results indicate significant differences between formulations ($p < 0.05$).

Rhim *et al.* [56] in PLA/soy protein/PLA isolate multilayer films and Rocca-Smith *et al.* [7] in PLA/wheat gluten/PLA systems. Regarding the effect of YMNs, it can be seen in Figure 11a that the addition of the yerba mate nanoparticles to one of the PLA layers led to a significant decrease in the oxygen permeability of the samples. This behavior can be explained by the synergic effect of nanoparticles to increase the tortuosity of the diffusion path of oxygen through the polymer and the tri-layer structures, thus considerably reducing the permeability [59]. Moreover, the well-known antioxidant properties of YMNs can provide some oxygen scavenging capacity, thus contributing to further reducing the oxygen permeability [21, 60, 61]. It should be highlighted that one of the major drawbacks of PLA-based materials for food packaging applications is its low oxygen barrier performance. The results obtained here showed that the middle layer of caseinate could improve the oxygen barrier performance of PLA in the tri-layer structure, thus, suggesting that the multilayer films developed here could be suitable for food packaging applications with reduced oxygen permeation.

Another agent with a pernicious effect on food packaging is moisture. Figure 11b displays the *WVP* values of the different monolayer and tri-layer film samples. In the case of RPLA, the obtained value is similar to that previously reported for this polymer [29]. Similarly, the *WVP* value obtained for the glycerol plasticized sodium caseinate film is in good agreement with that previously published in several studies [62–64]. The significantly higher *WVP* of the sodium caseinate layer can be attributed to the hydrophilic character of the sodium caseinate matrix, which facilitates the water vapor transport across the material. The inclusion of the caseinate layer between the RPLA layers led to an improvement of the barrier properties against water vapor due to the hydrophobic PLA layers protecting the inner caseinate layer. Similar results have been reported by Trinh *et al.* [65] in PLA/thermoplastic starch/PLA multilayer films, in which the PLA layers helped to reduce the *WVP* of the hydrophilic starch layer. Rocca-Smith *et al.* [7] also pointed out the positive effect on *WVP* of external PLA layers in PLA/wheat gluten/PLA multilayer films, allowing for improving the barrier properties of the internal hydrophilic gluten layer.

Specific migration tests were conducted to assess the release of antioxidant compounds from the YMNs contained in the inner layer of the tri-layer formulations. Tri-layer formulations were exposed to a fatty food simulant D1, particularly the inner active layer was in direct contact with the food simulant. The released compounds into the food simulant D1 were assessed by DPPH method, with the main objective of determining the antioxidant ability of the developed tri-layer films. As expected, a significantly ($p < 0.05$) greater antioxidant effectiveness was detected in the formulation with a higher content of YMNs, that is RPLA/SC/RPLA-YMN3 (81.1 ± 2.5 GA mg/dm^2 film) than in that with the lowest amount used here of 1 wt% of YMNs (RPLA/SC/RPLA-YMN1 = 36.8 ± 2.5 GA mg/dm^2 film). The antioxidant activity can be improved due to the presence of shorter PLA chains, such as oligomers produced during the mechanical recycling process, that can further act as plasticizers for RPLA matrix. It is known that plasticizers are able to improve the release capacity of active compounds from the polymeric matrix to the foodstuff [13, 66]. In fact, in previous work, it has been observed that PLA-based formulations plasticized with oligomeric lactic acid (OLA) showed higher antioxidant effectiveness than unplasticized ones [13]. Deladino *et al.* [26] studied different starch-based polymeric matrices as the carrier of yerba mate extract in different loading levels (from 9 to 50 wt%) and found starch-yerba mate based systems with very good antioxidant activity, such as DPPH inhibition of around 50% for the lowest amount of yerba mate extract used and more than 80% of inhibition for the sample with 50 wt% of yerba mate extract. Our results are in good agreement with that of Deladino *et al.* [26], considering the lowest loading levels (RPLA/SC/RPLA-YMN = 6.4 ± 0.1% of radical scavenging inhibition and RPLA/SC/RPLA-YMN3 = 11.0 ± 0.2% of radical scavenging inhibition).

Since each reprocessing cycle deleteriously affects the thermomechanical performance of PLA matrix, PLA-based materials cannot be infinitely recycled [8, 67]. Fortunately, recycled PLA-based materials can be composted under industrial composting conditions after their useful life in the same way as single-use PLA-based materials [9, 11]. Therefore, the tri-layer formulations were submitted to a disintegrability test in a composting medium at a laboratory scale level. Figure 12a shows the visual appearance of tri-layer films during composting, while Figure 12b is represented the degree of disintegration as a function of time. In only 4 days of disintegration under
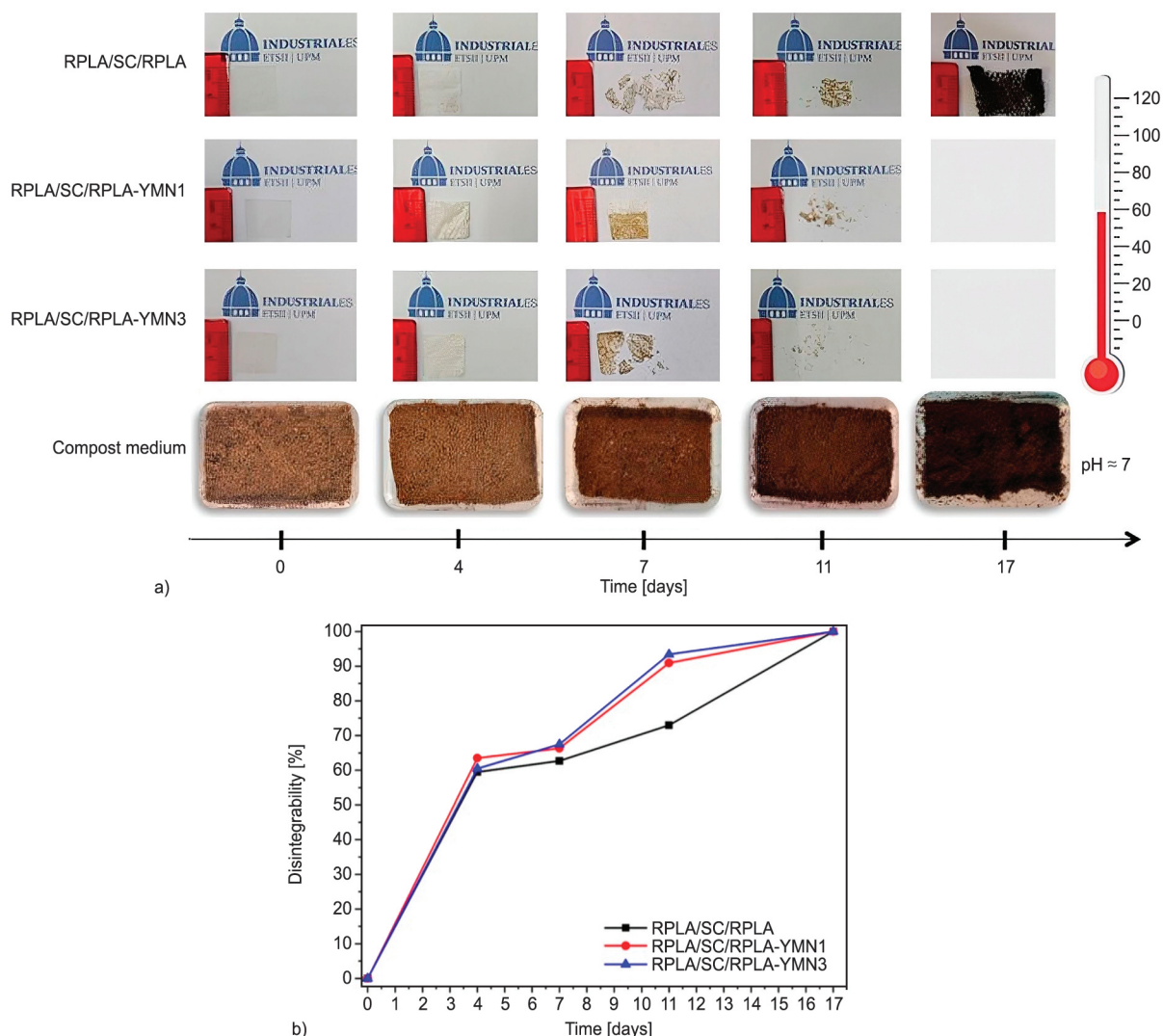
Figure 12. Disintegrability under composting conditions: a) visual appearance of tri-layer films before and after different composting days, b) tri-layer films disintegration degree [%] as a function of time [days].

composting, the materials lost a considerable amount of their initial mass (around 60%, Figure 12b) accompanied by evident macroscopic changes, such as reduced transparency (Figure 12a). It has been reported that SC monolayer films were fully disintegrated under composting conditions in 6 h, as sodium caseinate is soluble in water [68], but the main disintegration process of the protein does not start until glycerol was completely released [68, 69]. The obtained results suggest that a considerable amount of SC layer was lost during the 4 first days of the composting test. Then, after 7 days under composting conditions, the disintegration rate of tri-layer films slowed down, and a somewhat higher disintegration rate for tri-layer systems composed of the nanocomposite layer was observed.

It also could be noticed that RPLA/SC/RPLA-YMN1 and RPLA/SC/RPLA-YMN3 changed their color

and acquired a brownish tonality. The changes in the color and the increased opacity could indicate that a water uptake process takes place and/or the existence of products formed during the hydrolytic degradation process of the RPLA polymeric matrix, which induces a change in the refraction index of the polymeric films [38, 70]. On the 11th day of the composting test, both tri-layer systems composed of a YMNs reinforced RPLA layer reached 90% of weight loss, which is frequently used as the goal of the disintegrability test [38, 71]. The hydrophilic nature of YMNs favors the water penetration into the extremely disintegrated polymeric matrix at this stage. Meanwhile, RPLA/SC/RPLA formulation completely disappeared in 17 days. The success of the compostability experiment was followed by the evolution of the change of compost soil's visual appearance, which finally resulted in humus-rich soil (Figure 12a) with a pH of 7.1.

4. Conclusions

Tri-layer films of two external layers of mechanically recycled PLA and an intermediate layer of glycerol plasticized sodium caseinate were successfully produced by compression molding process without the need of adding adhesives or chemically modifying the film surface. Additionally, the inner layer of PLA was loaded with different content of lignocellulosic nanoparticles, extracted from yerba mate waste (YMNs). A cationic surfactant was used to improve the dispersion of YMNs into the recycled PLA polymeric matrix. The structural analysis and the morphological observation, together with the barrier and mechanical characterization allows suggesting the existence of hydrogen interactions between PLA and caseinate polymeric layers at the interface. The addition of YMNs into the inner layer of the tri-layer formulation contributed to improving the oxygen barrier properties of the tri-layer films, at the same time providing the formulation antioxidant activity that could lead to tri-layer films interesting for active food packaging applications. Meanwhile, although the PLA outer layers were able to protect the caseinate internal layer from water, the WVP values were worst than that of neat PLA but considerably better than neat sodium caseinate film. The tri-layer structure also had beneficial effects on the mechanical properties of the films, evidenced by the governing effect of PLA mechanical behavior. Additionally, the tri-layer films were fully disintegrated under composting conditions in less than 20 days, highlighting the suitability of these RPLA-based tri-layer polymeric structures for biodegradable active food packaging applications toward a circular bioeconomy.

References

[1] Auras R., Harte B., Selke S.: An overview of polylactides as packaging materials. Macromolecular Bioscience, **4**, 835–864 (2004).
https://doi.org/10.1002/mabi.200400043

[2] Armentano I., Bitinis N., Fortunati E., Mattioli S., Rescignano N., Verdejo R., López-Manchado M. A., Kenny J. M.: Multifunctional nanostructured PLA materials for packaging and tissue engineering. Progress in Polymer Science, **38**, 1720–1747 (2013).
https://doi.org/10.1016/j.progpolymsci.2013.05.010

[3] Benbettaïeb N., Debeaufort F., Karbowiak T.: Bioactive edible films for food applications: Mechanisms of antimicrobial and antioxidant activity. Critical Reviews in Food Science and Nutrition, **59**, 3431–3455 (2019).
https://doi.org/10.1080/10408398.2018.1494132

[4] Raquez J-M., Habibi Y., Murariu M., Dubois P.: Polylactide (PLA)-based nanocomposites. Progress in Polymer Science, **38**, 1504–1542 (2013).
https://doi.org/10.1016/j.progpolymsci.2013.05.014

[5] Lim L-T., Auras R., Rubino M.: Processing technologies for poly(lactic acid). Progress in Polymer Science, **33**, 820–852 (2008).
https://doi.org/10.1016/j.progpolymsci.2008.05.004

[6] Arrieta M. P., Samper M. D., Aldas M., López J.: On the use of PLA-PHB blends for sustainable food packaging applications. Materials, **10**, 1008–1034 (2017).
https://doi.org/10.3390/ma10091008

[7] Rocca-Smith J. R., Pasquarelli R., Lagorce-Tachon A., Rousseau J., Fontaine S., Aguié-Béghin V., Debeaufort F., Karbowiak T.: Toward sustainable PLA-based multilayer complexes with improved barrier properties. ACS Sustainable Chemistry and Engineering, **7**, 3759–3771 (2019).
https://doi.org/10.1021/acssuschemeng.8b04064

[8] Badia J. D., Santonja-Blasco L., Martínez-Felipe A., Ribes-Greus A.: Reprocessed polylactide: Studies of thermo-oxidative decomposition. Bioresource Technology, **114**, 622–628 (2012).
https://doi.org/10.1016/j.biortech.2012.02.128

[9] Beltrán F. R., Arrieta M. P., Moreno E., Gaspar G., Muneta L. M., Carrasco-Gallego R., Yañez S., Hidalgo-Carvajal D., de la Orden M. U., Martínez-Urreaga J.: Evaluation of the technical viability of distributed mechanical recycling of PLA 3D printing wastes. Polymers, **13**, 1247–1269 (2021).
https://doi.org/10.3390/polym13081247

[10] Beltrán F. R., Lorenzo V., de la Orden M. U., Martínez-Urreaga J.: Effect of different mechanical recycling processes on the hydrolytic degradation of poly(L-lactic acid). Polymer Degradation and Stability, **133**, 339–348 (2016).
https://doi.org/10.1016/j.polymdegradstab.2016.09.018

[11] Beltrán F. R., Arrieta M. P., Antón D. E., Lozano-Pérez A. A., Cenis J. L., Gaspar G., de la Orden M. U., Martínez-Urreaga J.: Effect of yerba mate and silk fibroin nanoparticles on the migration properties in ethanolic food simulants and composting disintegrability of recycled PLA nanocomposites. Polymers, **13**, 1925–1946 (2021).
https://doi.org/10.3390/polym13121925

[12] Beltrán F. R., de la Orden M. U., Lorenzo V., Pérez E., Cerrada M. L., Martínez Urreaga J.: Water-induced structural changes in poly(lactic acid) and PLLA-clay nanocomposites. Polymer, **107**, 211–222 (2016).
https://doi.org/10.1016/j.polymer.2016.11.031

[13] Arrieta M. P., García A. D., López D., Fiori S., Peponi L.: Antioxidant bilayers based on PHBV and plasticized electrospun PLA-PHB fibers encapsulating catechin. Nanomaterials, **9**, 346–360 (2019).
https://doi.org/10.3390/nano9030346

[14] Martucci J. F., Ruseckaite R. A.: Three-layer sheets based on gelatin and poly(lactic acid), Part 1: Preparation and properties. Journal of Applied Polymer Science, **118**, 3102–3110 (2010).
https://doi.org/10.1002/app.32751

[15] Rhim J-W., Lee J. H., Ng P. K. W.: Mechanical and barrier properties of biodegradable soy protein isolate-based films coated with polylactic acid. LWT – Food Science and Technology, **40**, 232–238 (2007).
https://doi.org/10.1016/j.lwt.2005.10.002

[16] Pereda M., Aranguren M. I., Marcovich N. E.: Characterization of chitosan/caseinate films. Journal of Applied Polymer Science, **107**, 1080–1090 (2008).
https://doi.org/10.1002/app.27052

[17] Arrieta M. P., Peltzer M. A., López J., del Camen Garrigós M., Valente A. J. M., Jiménez A.: Functional properties of sodium and calcium caseinate antimicrobial active films containing carvacrol. Journal of Food Engineering, **121**, 94–101 (2014).
https://doi.org/10.1016/j.jfoodeng.2013.08.015

[18] Khan M. R., Volpe S., Valentino M., Miele N. A., Cavella S., Torrieri E.: Active casein coatings and films for perishable foods: Structural properties and shelf-life extension. Coatings, **11**, 899–918 (2021).
https://doi.org/10.3390/coatings11080899

[19] Kristo E., Biliaderis C. G., Zampraka A.: Water vapour barrier and tensile properties of composite caseinate-pullulan films: Biopolymer composition effects and impact of beeswax lamination. Food Chemistry, **101**, 753–764 (2007).
https://doi.org/10.1016/j.foodchem.2006.02.030

[20] Rojas-Lema S., Torres-Giner S., Quiles-Carrillo L., Gomez-Caturla J., Garcia-Garcia D., Balart R.: On the use of phenolic compounds present in citrus fruits and grapes as natural antioxidants for thermo-compressed bio-based high-density polyethylene films. Antioxidants, **10**, 14–37 (2021).
https://doi.org/10.3390/antiox10010014

[21] Arrieta M. P., de Dicastillo C. L., Garrido L., Roa K., Galotto M. J.: Electrospun PVA fibers loaded with antioxidant fillers extracted from *Durvillaea antarctica* algae and their effect on plasticized PLA bionanocomposites. European Polymer Journal, **103**, 145–157 (2018).
https://doi.org/10.1016/j.eurpolymj.2018.04.012

[22] Luzi F., Pannucci E., Clemente M., Grande E., Urciuoli S., Romani A., Torre L., Puglia D., Bernini R., Santi L.: Hydroxytyrosol and oleuropein-enriched extracts obtained from olive oil wastes and by-products as active antioxidant ingredients for poly(vinyl alcohol)-based films. Molecules, **26**, 2104–2034 (2021).
https://doi.org/10.3390/molecules26072104

[23] Holowaty S. A., Thea A. E., Alegre C., Schmalko M. E.: Differences in physicochemical properties of yerba maté (*Ilex paraguariensis*) obtained using traditional and alternative manufacturing methods. Journal of Food Process Engineering, **41**, e12911 (2018).
https://doi.org/10.1111/jfpe.12911

[24] Arrieta M. P., Peponi L., López D., Fernández-García M.: Recovery of yerba mate (*Ilex paraguariensis*) residue for the development of PLA-based bionanocomposite films. Industrial Crops and Products, **111**, 317–328 (2018).
https://doi.org/10.1016/j.indcrop.2017.10.042

[25] Dahlem M. A., Borsoi C., Hansen B., Catto A. L.: Evaluation of different methods for extraction of nanocellulose from yerba mate residues. Carbohydrate Polymers, **218**, 78–86 (2019).
https://doi.org/10.1016/j.carbpol.2019.04.064

[26] Deladino L., Teixeira A. S., Navarro A. S., Alvarez I., Molina-García A. D., Martino M.: Corn starch systems as carriers for yerba mate (*Ilex paraguariensis*) antioxidants. Food and Bioproducts Processing, **94**, 463–472 (2015).
https://doi.org/10.1016/j.fbp.2014.07.001

[27] Nunes Ferraz Júnior A. D., Etchelet M. I., Braga A. F. M., Clavijo L., Loaces I., Noya F., Etchebehere C.: Alkaline pretreatment of yerba mate (*Ilex paraguariensis*) waste for unlocking low-cost cellulosic biofuel. Fuel, **266**, 117068 (2020).
https://doi.org/10.1016/j.fuel.2020.117068

[28] Correa V. G., Gonçalves G. A., de Sá-Nakanishi A. B., Ferreira I. C., Barros L., Dias M. I., Koehnlein E. A., de Souza C. G. M., Bracht A., Peralta R. M.: Effects of *in vitro* digestion and *in vitro* colonic fermentation on stability and functional properties of yerba mate (*Ilex paraguariensis* A. St. Hil.) beverages. Food Chemistry, **237**, 453–460 (2017).
https://doi.org/10.1016/j.foodchem.2017.05.125

[29] Beltrán F. R., Arrieta M. P., Gaspar G., de la Orden M. U., Urreaga J. M.: Effect of lignocellulosic nanoparticles extracted from yerba mate (*Ilex paraguariensis*) on the structural, thermal, optical and barrier properties of mechanically recycled poly(lactic acid). Polymers, **12**, 1690–1710 (2020).
https://doi.org/10.3390/polym12081690

[30] Arrieta M. P., Fortunati E., Burgos N., Peltzer M. A., López J., Peponi L.: Nanocellulose-based polymeric blends for food packaging applications. in 'Multifunctional polymeric nanocomposites based on cellulosic reinforcements' (eds.: Puglia D., Fortunati E., Kenny J. M.) Elsevier, Oxford, 205–252 (2016).

[31] Fortunati E., Armentano I., Zhou Q., Iannoni A., Saino E., Visai L., Berglund L. A., Kenny J. M.: Multifunctional bionanocomposite films of poly(lactic acid), cellulose nanocrystals and silver nanoparticles. Carbohydrate Polymers, **87**, 1596–1605 (2012).
https://doi.org/10.1016/j.carbpol.2011.09.066

[32] Luzi F., Fortunati E., Jiménez A., Puglia D., Chiralt A., Torre L.: PLA nanocomposites reinforced with cellulose nanocrystals from *Posidonia oceanica* and ZnO nanoparticles for packaging application. Journal of Renewable Materials, **5**, 103–115 (2017).
https://doi.org/10.7569/JRM.2016.634135

[33] Sessini V., Navarro-Baena I., Arrieta M. P., Dominici F., López D., Torre L., Kenny J. M., Dubois P., Raquez J-M., Peponi L.: Effect of the addition of polyester-grafted-cellulose nanocrystals on the shape memory properties of biodegradable PLA/PCL nanocomposites. Polymer Degradation and Stability, **152**, 126–138 (2018).
https://doi.org/10.1016/j.polymdegradstab.2018.04.012

[34] Cherpinski A., Gozutok M., Sasmazel H. T., Torres-Giner S., Lagaron J. M.: Electrospun oxygen scavenging films of poly(3-hydroxybutyrate) containing palladium nanoparticles for active packaging applications. Nanomaterials, **8**, 469–488 (2018).
https://doi.org/10.3390/nano8070469

[35] Capron I, Rojas O. J., Bordes R. Behavior of nanocelluloses at interfaces. Current Opinion in Colloid & Interface Science, **29**, 83–95 (2017).
https://doi.org/10.1016/j.cocis.2017.04.001

[36] Arrieta M. P., Peltzer M. A., del Carmen Garrigós M., Jiménez A.: Structure and mechanical properties of sodium and calcium caseinate edible active films with carvacrol. Journal of Food Engineering, **114**, 486–494 (2013).
https://doi.org/10.1016/j.jfoodeng.2012.09.002

[37] Beltrán F. R., Lorenzo V., Acosta J., de la Orden M. U., Martínez-Urreaga J. M.: Effect of simulated mechanical recycling processes on the structure and properties of poly(lactic acid). Journal of Environmental Management, **216**, 25–31 (2018).
https://doi.org/10.1016/j.jenvman.2017.05.020

[38] Arrieta M. P., Fortunati E., Dominici F., Rayón E., López J., Kenny J. M.: PLA-PHB/cellulose based films: Mechanical, barrier and disintegration properties. Polymer Degradation and Stability, **107**, 139–149 (2014).
https://doi.org/10.1016/j.polymdegradstab.2014.05.010

[39] UNE EN-ISO 13468-1:2019: Plastics – Determination of the total luminous transmittance of transparent materials – Part 1: Single-beam instrument (2019).

[40] Arranz-Andrés J., Lorenzo V., de la Orden M. U., Pérez E., Cerrada M. L.: Tailoring transport properties in blends based on olephinic and liquid crystalline polymers. Journal of Membrane Science, **377**, 141–150 (2011).
https://doi.org/10.1016/j.memsci.2011.04.023

[41] ISO 2528:2017: Determination of water vapour transmission rate (WVTR) – Gravimetric (dish) method (2017).

[42] UNE EN-ISO 20200:2015: Determination of the degree of disintegration of plastic materials under simulated composting conditions in a laboratory-scale test (2016).

[43] Mondragon G., Fernandes S., Retegi A., Peña C., Algar I., Eceiza A., Arbelaiz A.: A common strategy to extracting cellulose nanoentities from different plants. Industrial Crops and Products, **55**, 140–148 (2014).
https://doi.org/10.1016/j.indcrop.2014.02.014

[44] de Souza A. G., de Lima G. F., Colombo R., Rosa D. S.: A new approach for the use of anionic surfactants: Nanocellulose modification and development of biodegradable nanocomposites. Cellulose, **27**, 5707–5728 (2020)
https://doi.org/10.1007/s10570-020-03160-3

[45] Campbell R. A., Parker S. R., Day J. P., Bain C. D.: External reflection FTIR spectroscopy of the cationic surfactant hexadecyltrimethylammonium bromide (CTAB) on an overflowing cylinder. Langmuir, **20**, 8740–8753 (2004).
https://doi.org/10.1021/la048680x

[46] Chariyachotilert C., Joshi S., Selke S. E., Auras R.: Assessment of the properties of poly(L-lactic acid) sheets produced with differing amounts of postconsumer recycled poly(L-lactic acid). Journal of Plastic Film and Sheeting, **28**, 314–335 (2012).
https://doi.org/10.1177/8756087911434337

[47] Beltrán F., de la Orden M. U., Martínez-Urreaga J. M.: Amino-modified halloysite nanotubes to reduce polymer degradation and improve the performance of mechanically recycled poly(lactic acid). Journal of Polymers and the Environment, **26**, 4046–4055 (2018).
https://doi.org/10.1007/s10924-018-1276-6

[48] di Lorenzo M. L.: Calorimetric analysis of the multiple melting behavior of poly(L-lactic acid). Journal of Applied Polymer Science, **100**, 3145–3151 (2006).
https://doi.org/10.1002/app.23136

[49] Gordobil O., Egüés I., Llano-Ponte R., Labidi J.: Physicochemical properties of PLA lignin blends. Polymer Degradation and Stability, **108**, 330–338 (2014).
https://doi.org/10.1016/j.polymdegradstab.2014.01.002

[50] Bužarovska A., Blazevska-Gilev J., Pérez-Martnez B. T., Balahura L. R., Pircalabioru G. G., Dinescu S., Costache M.: Poly(L-lactic acid)/alkali lignin composites: Properties, biocompatibility, cytotoxicity and antimicrobial behavior. Journal of Materials Science, **56**, 13785–13800 (2021).
https://doi.org/10.1007/s10853-021-06185-6

[51] Szép A., Marosfői B., Bertalan G., Anna P., Marosi G.: Analysis of multicomponent polymer systems by Raman microscopy. Macromolecular Symposia, **202**, 269–280 (2003).
https://doi.org/10.1002/masy.200351223

[52] Widjaja E., Garland M.: Reverse engineering of multi-layer films. Materials Today, **14**, 114–117 (2011).
https://doi.org/10.1016/S1369-7021(11)70061-X

[53] Larkin P.: Infrared and Raman spectroscopy: Principles and spectral interpretation. Elsevier, San Diego (2017).

[54] Qin D., Kean R. T.: Crystallinity determination of poly-lactide by FT-Raman spectrometry. Applied Spectroscopy, **52**, 488–495 (1998).
https://doi.org/10.1366/0003702981943950

[55] Zhuang Y., Sterr J., Kulozik U., Gebhardt R.: Application of confocal Raman microscopy to investigate casein micro-particles in blend casein/pectin films. International Journal of Biological Macromolecules, **74**, 44–48 (2015).
https://doi.org/10.1016/j.ijbiomac.2014.11.017

[56] Rhim J-W., Mohanty K. A., Singh S. P., Ng P. K. W.: Preparation and properties of biodegradable multilayer films based on soy protein isolate and poly(lactide). Industrial and Engineering Chemistry Research, **45**, 3059–3066 (2006).
https://doi.org/10.1021/ie051207

[57] Ramos M., Arrieta M. P., Beltran A., Garrigós M. C.: Characterization of PLA, PCL and sodium caseinate active bio-films for food packaging applications. in 'Food packaging: Procedures, management and trends' (ed: Kontominas M.) Nova Science, New York, 63–78 (2012).

[58] Tomasula P. M., Yee W. C., Parris N.: Oxygen permeability of films made from CO_2-precipitated casein and modified casein. Journal of Agricultural and Food Chemistry, **51**, 634–639 (2003).
https://doi.org/10.1021/jf020552w

[59] Choudalakis G., Gotsis A. D.: Permeability of polymer/clay nanocomposites: A review. European Polymer Journal, **45**, 967–984 (2009).
https://doi.org/10.1016/j.eurpolymj.2009.01.027

[60] Muller J., González-Martínez C., Chiralt A.: Poly(lactic) acid (PLA) and starch bilayer films, containing cinnamaldehyde, obtained by compression moulding. European Polymer Journal, **95**, 56–70 (2017).
https://doi.org/10.1016/j.eurpolymj.2017.07.019

[61] Bonilla J., Talón E., Atarés L., Vargas M., Chiralt A.: Effect of the incorporation of antioxidants on physico-chemical and antioxidant properties of wheat starch–chitosan films. Journal of Food Engineering, **118**, 271–278 (2013).
https://doi.org/10.1016/j.jfoodeng.2013.04.008

[62] Khwaldia K., Banon S., Perez C., Desobry S.: Properties of sodium caseinate film-forming dispersions and films. Journal of Dairy Science, **87**, 2011–2016 (2004).
https://doi.org/10.3168/jds.S0022-0302(04)70018-1

[63] Kristo E., Koutsoumanis K. P., Biliaderis C. G.: Thermal, mechanical and water vapor barrier properties of sodium caseinate films containing antimicrobials and their inhibitory action on Listeria monocytogenes. Food Hydrocolloids, **22**, 373–386 (2008).
https://doi.org/10.1016/j.foodhyd.2006.12.003

[64] Aliheidari N., Fazaeli M., Ahmadi R., Ghasemlou M., Emam-Djomeh Z.: Comparative evaluation on fatty acid and *Matricaria recutita* essential oil incorporated into casein-based film. International Journal of Biological Macromolecules, **56**, 69–75 (2013).
https://doi.org/10.1016/j.ijbiomac.2013.02.007

[65] Trinh B. M., Chang C. C., Mekonnen T. H.: Facile fabrication of thermoplastic starch/poly(lactic acid) multilayer films with superior gas and moisture barrier properties. Polymer, **223**, 123679–123692 (2021).
https://doi.org/10.1016/j.polymer.2021.123679

[66] del Mar Castro López M., de Dicastillo C. L., Vilarino J. M. L., Rodríguez M. V. G.: Improving the capacity of polypropylene to be used in antioxidant active films: Incorporation of plasticizer and natural antioxidants. Journal of Agricultural and Food Chemistry, **61**, 8462–8470 (2013).
https://doi.org/10.1021/jf402670a

[67] Agüero A., del Carmen Morcillo M., Quiles-Carrillo L., Balart R., Boronat T., Lascano D., T. Torres Giner S., Fenollar O.: Study of the influence of the reprocessing cycles on the final properties of polylactide pieces obtained by injection molding. Polymers, **11**, 1908–1929 (2019).
https://doi.org/10.3390/polym11121908

[68] Arrieta M. P., Peltzer M. A., Garrigos M. C., Jiménez A.: Antibacterial biofilms based on calcium caseinate incorporated with carvacrol. in 'Microbes in applied research' (ed.: Mendez-Vilas A.) World Scientific, Singapore, 469–473 (2011).
https://doi.org/10.1142/9789814405041_0095

[69] Martucci J. F., Ruseckaite R. A.: Biodegradation behavior of three-layer sheets based on gelatin and poly(lactic acid) buried under indoor soil conditions. Polymer Degradation and Stability, **116**, 36–44 (2015).
https://doi.org/10.1016/j.polymdegradstab.2015.03.005

[70] Iglesias-Montes M. L., Luzi F., Dominici F., Torre L., Manfredi L. B., Cyras V. P., Puglia D.: Migration and degradation in composting environment of active polylactic acid bilayer nanocomposites films: Combined role of umbelliferone, lignin and cellulose nanostructures. Polymers, **13**, 282–297 (2021).
https://doi.org/10.3390/polym13020282

[71] Luzi F., Fortunati E., Jiménez A., Puglia D., Pezzolla D., Gigliotti G., Kenny J. M., Chilart A., Torre L.: Production and characterization of PLA_PBS biodegradable blends reinforced with cellulose nanocrystals extracted from hemp fibres. Industrial Crops and Products, **93**, 276–289 (2016).
https://doi.org/10.1016/j.indcrop.2016.01.045